Nineteenth Australasian Wind Engineering Society Workshop, April 4-6, 2018, Torquay, Victoria

Antenna Shielding on Monopole Structures - Part 1 Experimental

Tom Moyle[1], Neil Mackenzie[2], Richard Jones[3]
[1]*Aurecon Group, Adelaide, SA, thomas.moyle@aurecongroup.com*
[2]*Aurecon Group, Adelaide, SA,* neil.mackenzie@aurecongroup.com
[3]*Aurecon Group, Adelaide, SA, richard.jones@aurecongroup.com*

ABSTRACT

Telstra's portfolio of antenna support structures is facing increasing loads due to implementation of additional technologies and headframe mounted equipment. As a result, Telstra's costs associated with upgrade or swap out of existing structures is increasing. This paper will outline the experimental study undertaken by Aurecon which investigated antenna shielding on headframes. Effective sail areas (ESA) for a suite of headframe and antenna configurations were determined from wind tunnel tests. These ESAs have been included in an update of the "Deployment Rules for Telstra Antenna Support Structures", ensuring a consistent approach to antenna shielding is taken by Telstra's structural contractors. This paper will discuss the experimental component of this study.

1. Introduction

In 2015, Telstra approved the use of antenna shielding in the calculation of headframe load (Armour, 2015). However, the ESA data available was limited and dated; based on old technology and configurations pre-Remote Radio Unit (RRU) deployment. Aurecon were engaged to develop a calibrated computational approach to determine a headframe's ESA, updating and extending Woods' (2007) previous research. The study involved wind tunnel testing of seven different headframe types in over 40 different configurations and using this experimental data to calibrate a computational fluid dynamics (CFD) method. The study culminated in an update of the "Deployment Rules for Telstra Antenna Support Structures". This is a two-part paper, with "Antenna Shielding on Monopole Structures - Part 2 Computational" (Moyle et al., 2018) providing a discussion of the CFD method and related findings.

2. Experimental Method

2.1 Model Construction

Seven headframes were included in the study, the M1 (with and without cross arms), Rocla, Circular, Lattice, J1/J2, Square, and Mercedes. The effect of RRU Mounts and other ancillary components including cable trays and feeder cables were also studied. All the headframes were constructed at 1:5 scale using aluminium and 3D printed plastic components. Components attached to the headframes were constructed from foam with a MDF backing, wrapped in 40 grit sandpaper ($425\mu m$ particles). The increase in surface roughness was necessary to ensure a transition from a laminar to turbulent boundary layer flow at a lower Reynolds number than if the surface was smooth, mimicking the flow field behaviour at higher Reynolds numbers. At 1:5 scale the geometry of all components was approximated as sharp edged rectangular bodies, except for the larger RVVPX310 antenna where a radius of approximately 8mm was achieved with the sandpapered surface. Several configurations were also tested with feeder cables in an attempt to quantify their drag contribution. The headframe poles were approximately 600mm high, ensuring the headframes were in the wind tunnel's uniform flow region. Figure 1 shows the M1 (with cross arms) and Circular headframes, and the RRU mounts installed in the wind tunnel for one of their respective antenna configurations.

Single antenna were also tested to qualify their performance relative to code and manufacturer claims. These were tested at a variety of scales dependent on antenna geometry.

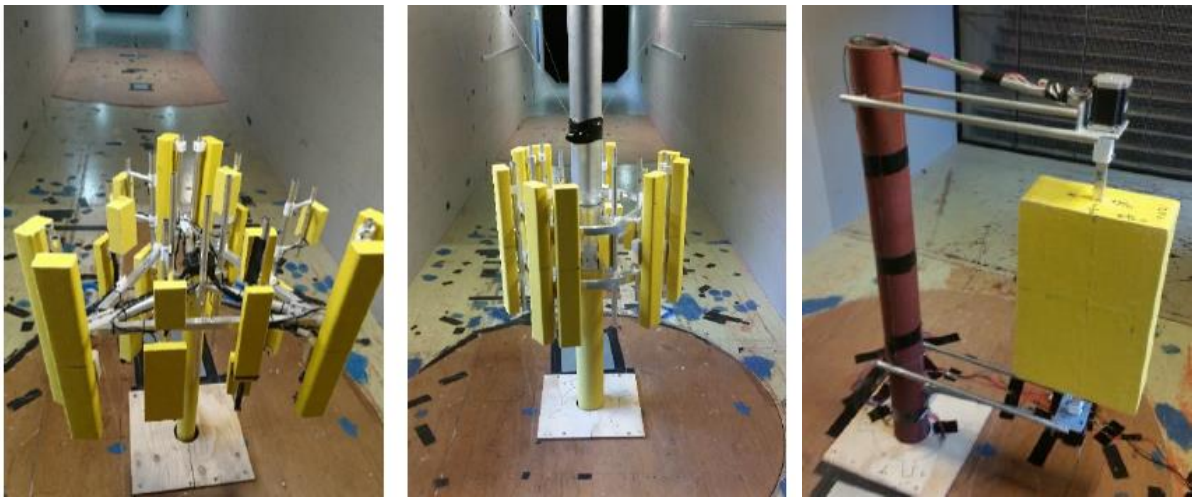

Figure 1: [Left] - M1 headframe with cross arms in the showcase configuration with cables; [Centre] – Circle headframe in the showcase configuration with the upper pole; [Right] – The MM-WAVE antenna mounted on the instrumented test rig.

2.2 Tunnel Equipment & Configuration

Measurements were carried out at Monash University's closed loop 450kW wind tunnel using a high frequency force balance (HFFB). The tunnel has a cross sectional area of 4m^2 and a development length of approximately 12m. This tunnel's test section does not have louvred-relief; correction of wake and solid blockage effects is discussed in Section 4.2. Wind force measurements were taken at 10° increments for all headframe configurations and individual antenna. Symmetric geometry (about 90° and 120°) was exploited to reduce the total number of tests required. Several 360° measurements were also performed to evaluate hysteresis, variance from symmetry, and repeatability.

The flow had the following properties:

- The mean wind speed profile was uniform over the test section (within ±1%).
- The boundary layer height ranged from 200-400mm dependent on the freestream velocity.
- The freestream turbulence intensity was less than 1.2% over the chosen freestream velocities, for $z \geq 600$mm. The turbulence intensity has a maximum of 4% for 300mm $\leq z <$ 600mm.
- The flow angularity was ±1%.
- The horizontal boundary layer was approximately 400mm for freestream velocities greater than 10m/s.

An upper pole (Figure 1) was included in the measurements for headframes that can be located down the structure.

2.3 Vortex Shedding

The support pole material, length, and diameter were selected to ensure the structure was not excited at resonance due to vortex shedding. A configuration consisting of a rigid frame with two steppers was test the individual antenna. The rigid frame remained fixed in relation to the HFFB with the stepper motors controlling the antenna's yaw angle.

3. Analysis Method

3.1 Effective Sail Area

In accordance with telecommunication industry practice the ESA for each headframe configuration was calculated from the mean drag force where,

$$ESA(\theta) = \overline{C_d(t)A_d(\theta)} = \overline{\left(\frac{F_d(\theta,t)}{\frac{1}{2}\rho(t)V_\infty(t)}\right)} \quad (1)$$

$C_d(t)A_d(\theta)$ is the instantaneous drag force area, $F_d(\theta,t)$ is the drag force, $\rho(t)$ is the density of air, and $V_\infty(t)$ is the freestream velocity. The instantaneous drag force area was calculated from the F_x and F_y time series and averaged to give the ESA at a given yaw angle. The ESA's of the individual antenna were calculated from the moment about the z-axis.

3.2 Blockage Correction

During wind tunnel testing interference effects can occur if the ratio of the test specimen's frontal area to the tunnel's cross section is high. These effects have two contributing components, termed solid blockage and wake blockage.

Solid blockage occurs when the tunnel walls and the associated boundary layers restrict flow around the test specimen, causing localised flow acceleration (Hyvarinen, 2015). Solid blockage causes a symmetric pressure gradient about the test specimen, artificially increasing the measured drag.

Wake blockage occurs due to the development of a viscous wake behind the test specimen, further restricting the effective tunnel cross section, causing additional flow acceleration (Hyvarinen, 2015). Wake blockage may cause an asymmetrical pressure gradient, and result in an artificial drag increase.

Many studies have quantified the effects of wind tunnel interference and have detailed algorithms for correcting the recorded data (Rae and Pope, 1984). For this work the Maskell 3 blockage correction method for bluff bodies (Hackett and Cooper, 2001) has been implemented. The frontal area of the headframe was calculated for all test configurations, at all yaw angles. This was achieved by first creating a 3D digital model of the test configuration, together with a model of the wind tunnel cross-sectional area. Paraview's Python API was then used to generate black and white images of the model and wind tunnel, when viewed without perspective from the upstream direction. The model frontal area was then calculated by taking the ratio of black to white pixels in the image.

4. Results

Antenna headframes and masts are classified as bluff bodies with respect to the airflow around them. In bluff body aerodynamics, the most important parameters that affect the force coefficient are the bodies' geometry, edges, and curvature; Reynolds number of the flow; free-stream turbulence; and surface roughness ratio.

The analysis included a study on the effect of the Reynolds number and freestream turbulence, the uncertainty and repeatability of the wind tunnel measurements, and a comparison with code values. Further presentation of the experimental results is included in "Antenna Shielding on Monopole Structures - Part 2 Computational" for comparison with the CFD results.

4.1 Freestream Turbulence

When installed on-site, the headframe configurations will experience flow with turbulence intensity of several percent due to the atmospheric boundary layer and flow effects of the surrounding built environment. To quantify the effect of high turbulence intensity on the mean ESA a turbulence generating grid was mounted in the wind tunnel upstream of the test section, increasing the turbulence intensity to 7.5%. Only three headframe configurations were tested with a turbulence intensity of 7.5% as the approach flow was not adequately uniform. It was found that for the two

headframe configurations with few antenna and ancillary components the ESA decreased by up to 5.6% with increasing freestream turbulence intensity. The decrease in ESA with increasing freestream turbulence is an expected result as the Reynolds number is effectively increased. For a configuration with many antenna and ancillary components little change in the ESA was seen with increasing freestream turbulence. It is hypothesised that the complex geometry of the headframe configuration generated significant turbulence levels in the wake of the leading antennas. This led to self-generation of high ESA values with little influence due to the freestream turbulence levels.

4.2 Reynolds Number

To quantify the effect of the Reynolds number on the ESA, headframes were tested at freestream velocities of 10, 20 and 30m/s at 0° yaw. Several headframes were also tested at intermediate wind speeds where practical. It was found that the maximum change in ESA over the entire velocity range was 6.11%. Given the Reynolds number for the wind tunnel tests is already a factor of 5 lower than full scale, it is reasonable to exclude the lowest velocity 10m/s data since it is not representative of the Reynolds numbers of interest. When disregarding these values there is only a slight increase in ESA with freestream velocity of up to 1.67% across a factor of two change in Reynolds number.

4.3 Repeatability

Wind tunnel tests for one configuration were conducted twice to quantify repeatability. A difference of less than 0.3% was seen for all test angles, within the expected noise floor of the test method.

5.4 Code Comparison

Code comparisons were performed against AS1170.2 and EN 1991-1-4:2005+A1:E for the poles and individual components respectively.

Drag coefficients for cylindrical shapes are provided in Table E3 of the Australian Standard for wind actions, AS1170.2 (Standards Australia, 2011) and are intended to recreate the cylinder drag coefficient between the pre- and post-critical Reynolds number range. At pre-critical Reynolds numbers ($bV_{des,\theta} < 4\ m/s$) the drag coefficient is 1.2, while at post-critical Reynolds numbers ($bV_{des,\theta} > 10\ m/s$) the drag coefficient gradually increases from 0.6 as a function of velocity and surface roughness. Across the critical Reynolds number range ($4 < bV_{des,\theta} < 10\ m/s$) the drag coefficient is interpolated from 1.2 to 0.6.

On site the full-scale poles are expected to operate at post-critical Reynolds numbers where $bV_{des,\theta} \geq 10$ since $V_{des,\theta}$ is typically greater than 30m/s and b is 0.3m and 0.5m for the small and large poles respectively. However, at model scale $bV_{des,\theta} < 4$ for both configurations and the model poles are expected to be in the pre-critical Reynolds number range, leading to an expectation that $C_d = 1.2$ during wind tunnel testing. To counteract this, sandpaper surface roughness was used to artificially increase the Reynolds number behaviour of the fluid flow. It can be seen from the drag coefficients in Table 1 that both pole diameters show a minimum $C_d \approx 0.6$. The gradual increase in drag coefficient for the small pole at velocities greater than 20m/s indicates it is in the post-critical range, while the large pole appears to be in the post-critical range from velocities greater than 10m/s. This provides a strong indication that the sandpaper surface roughness effectively increases the model Reynolds number to reflect that expected of full scale tests.

A comparison between the wind tunnel results for the single antennas and EN 1991-1-4:2005+A1:E can be seen in Table 2. Agreement was strong for 0° yaw, but there were slight discrepancies between the experimental and code values at 90°.

Table 1: Wind tunnel ESA and C_d for poles at free stream velocities between 5 and 35m/s

Velocity (m/s)	60mm OD			100mm OD		
	Uncorrected ESA (m^2)	Blockage Corrected ESA (m^2)	Blockage Corrected C_d	Uncorrected ESA (m^2)	Blockage Corrected ESA (m^2)	Blockage Corrected C_d
5	0.77	0.76	0.81	1.06	1.03	0.66
10	0.64	0.63	0.67	1.00	0.98	0.63
15	0.58	0.57	0.61	1.05	1.02	0.65
20	0.56	0.55	0.59	1.03	1.00	0.64
25	0.61	0.60	0.64	1.07	1.04	0.67
30	0.62	0.61	0.65	1.08	1.05	0.67
35	0.64	0.63	0.67	1.09	1.06	0.68

Table 2: Comparison of the individual antenna's ESA from the wind tunnel and calculated using EN 1991-1-4:2005+A1:E (European Standard, 2010).

Config.	Height [mm]	Width [mm]	Depth [mm]	0°		90°	
				WT	Code	WT	Code
9.1	2533	350	208	1.29	1.23	0.71	0.52
9.2	1329	290	103	0.51	0.59	0.12	0.16
9.3	493	299	128	0.22	0.21	0.07	0.07
9.4	1200	475	120	0.84	0.81	-	0.13
9.5	586	306	178	0.31	0.28	0.17	0.12
9.6	380	160	180	0.11	0.09	0.09	0.10

5.6 Uncertainty

Sources of uncertainty in the wind tunnel to CFD comparison include:

- Wind tunnel models varying slightly to the CFD CAD models.
- Not achieving perfect symmetry of the wind tunnel model about the expected sectors of symmetry (e.g. 120° or 90° for the M1 and Square respectively) due to a combination of imperfections in the model and slight warping of the baseplate that occurred during the manufacture process.

The sources of uncertainty that occurred during wind tunnel testing are also expected to occur in real world headframe deployments with slight variations in headframe manufacturer, antenna deployment, cable tidiness etc. These sources of uncertainty are believed to typically sum to 2% of along-wind ESA, however they may be up to 5%. A safety factor of 10% (to account for further modelling uncertainties) has been applied to the ESA data provided in the update of the deployment rules.

5.7 Shielding

Shielding effects become more pronounced as the headframes approach a fully loaded configuration, this can be seen in Figure 2 for the J1/J2 headframe. The maximum ESA of the empty headframe (3.72m^2) almost doubles (6.26 m^2) with the addition of 6 antenna. However, for a configuration of 12 RVVPX310 antennas with 6 RRUs and 6 TMAs (tower mounted amplifier) (the

maximum number of antenna the J1/J2 headframe can accommodate) the maximum ESA increases to only 7.70m^2. This increase in ESA of 1.44m^2 when compared to the 6 antenna configuration is significantly less than the ESA of each additional antenna. For example, the ESA of one RVVPX310 at 0° yaw calculated using European Standard EN 1991-1-4:2005+A1:E (2010) is 1.23m^2. This provides opportunity for cost savings by avoiding strengthening and swap-out of existing structures with future technology deployments.

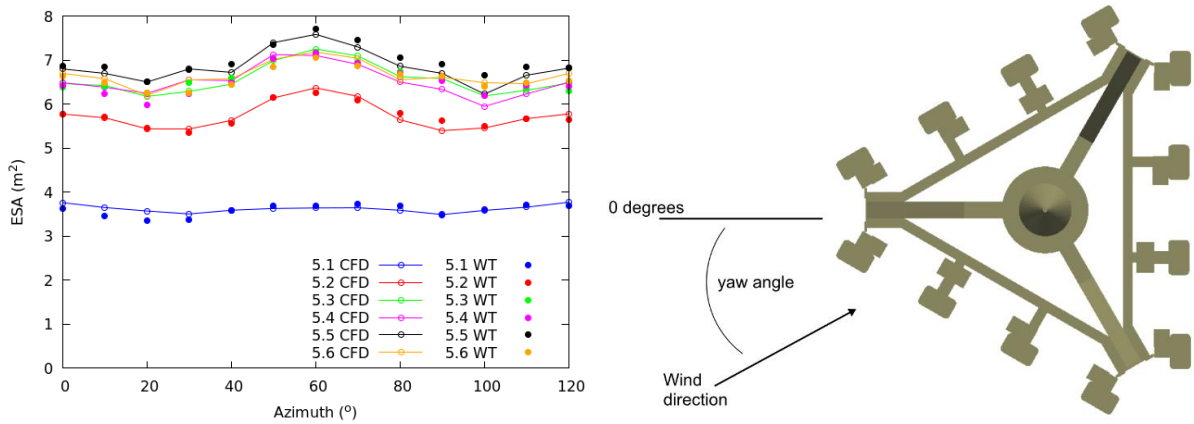

Figure 2: Left - J1/J2 configuration's ESA against azimuth angle; Right – Schematic diagram of the J1/J2.

6. Conclusions

The ESA of over 40 headframe and antenna configurations were determined experimentally. It was found that shielding effects can be significant with the addition of further antenna and components. The use of antenna shielding in structural certifications has significant positive implications for telecommunication providers by avoiding unnecessary strengthening or swap-out of existing structures with future technology deployments. This paper is continued in "Antenna Shielding on Monopole Structures - Part 2 Computational".

Acknowledgement

Aurecon would like to acknowledge our client, Telstra for the opportunity to carry out these works and present the findings of our research.

References

Armour, M., 2015, "016159 Deployment Rules for Telstra Antenna Support Structures", no. 10, AMJ-6429.

European Standard, 2010, "Eurocode 1: Actions on structures - Part 1-4: General actions - Wind actions". EN 1991-1-4:2005+A1:E.

Hackett, J.E., Cooper, K.R., 2001, "Extension to Maskell's Theory for Blockage Effects on Bluff Bodies in a Closed Wind Tunnel", The Aeronautical Journal, pp. 409-411.

Holmes, J.D, 2007, "Wind Loading of Structures", Taylor & Francis, 2nd edition, London and New York.

Hyvarinen, A., 2015, Investigation of blockage correction methods for full-scale wind tunnel testing of trucks, KTH Royal Institute of Technology.

Moyle, T., Mackenzie, N., Jones, R., 2018, "Antenna Shielding on Monopole Structures - Part 2 Computational", *Proceedings of the 19th Australian Wind Engineering Workshop.*

Rae, W.H. Pope, A, 1963, "Low-Speed Wind Tunnel Testing", John Wiley and Sons, 2nd edition, USA.

Standards Australia, 2011, "Structural design actions. Part 2 Wind actions", Australian/New Zealand Standard, AS/NZS 1170.2:2011.

Woods, G.S., 2007, "Wind Loading of Telecommunication Antennas and Head Frames", research report no. R881, The University of Sydney.